IEEE Access
Multidisciplinary | Rapid Review | Open Access Journal
SPECIAL SECTION ON ADVANCED ENERGY STORAGE TECHNOLOGIES AND THEIR APPLICATIONS

Received March 20, 2018, accepted April 25, 2018, date of publication April 30, 2018, date of current version June 19, 2018.

Digital Object Identifier 10.1109/ACCESS.2018.2831251

Passivity-Based Control Strategy for SMES Under an Unbalanced Voltage Condition

YONG LEI, XIAODONG LIN, AND YINGWEI ZHU
College of Electrical Engineering and Information Technology, Sichuan University, Chengdu 610065, China
Corresponding author: Yingwei Zhu (zhu-yingwei@163.com)

ABSTRACT This paper presents a novel nonlinear control strategy for a superconducting magnetic energy storage (SMES) system during network unbalance. Grid voltage unbalances tend to substantially degrade the operation of a SMES system; conventional control methods cannot completely address this issue. In this paper, three selectable control targets for the SMES are identified according to the working principle of the SMES under an unbalanced voltage condition to reduce the impacts of second harmonics in output power, output reactive power, and grid-side current. Next, the port-controlled Hamiltonian models of the SMES are established, and the positive- and negative-sequence interconnection and damping assignment passivity-based control (PBC) strategies are proposed accordingly. Simulation results show that the PBC has stronger robustness in both steady and dynamic states compared with the conventional proportional integral method, which effectively suppresses the oscillations caused by the unbalanced voltage.

INDEX TERMS IDA-PBC, network unbalance, port-controlled Hamiltonian, SMES.

I. INTRODUCTION

In recent years, with the exhaustion of traditional fossil-based energy sources and the aggravation of environmental pollution, new energy sources, including wind and solar power, have achieved rapid development. The energy storage of new energy sources plays a key role in improving power quality and enhancing power supply reliability [1], [2]. Of the various types of energy storage devices, superconducting magnetic energy storage (SMES) has attracted widespread attention due to its low dissipation of energy conversion, high power density, fast response and compatibility with a flexible installation location [3]–[8].

The energy storage converter of SMES is a complex system with nonlinear, strong coupling and multi-variable characteristics. The common control strategies of energy storage converters include proportional integral (PI) control [9], direct power control [10], sliding mode control [11], neural network control [12] and fuzzy control [13]. For the conventional PI method, many parameters must be tuned, and the performance of the PI method typically exhibits unsatisfactory robustness due to its local stability. For direct power control, inappropriate selection of the zero vector can result in the transient out-of-control situation of reactive power; thus, the establishment of the switch table requires further research [14]. Sliding mode control offers rapid dynamic response ability; however, high-frequency oscillation often occurs in the controlled variable [15]. The neural network control has a strong fault tolerance; however, the objective function can easily fall into a local minimum. The expert system in fuzzy control cannot define the control objective, and the steady-state accuracy of fuzzy control is low. The aforementioned control strategies neglect the internal and external interconnection structure of the nonlinear system and cannot be applied to an unbalanced voltage condition.

Under the unbalanced voltage condition, the energy storage converter of SMES outputs active power and reactive power containing second-harmonic ripple, which affects the steady-state operation of the system [16]–[18]. If no effective control strategy exists, then the unbalance grid voltage will greatly increase the loss of the energy storage converter and can even lead to the quenching of superconducting magnet; such quenching will seriously endanger the safe operation of the power grid. However, if the appropriate control strategy can be adopted for SMES converters, then the impact of the unbalance voltage on the operation of SMES can be compensated to a certain extent. Reference [19] proposed a control method for the rotor side converter of DFIG under the unbalanced voltage condition based on a two-phase static frame; the positive- and negative-sequence components are separated using band-trap filters to remove the oscillating terms and then controlled using two independent PID controllers. However, the anti-disturbance performance and dynamic response

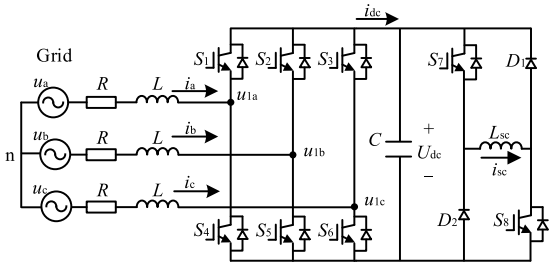

FIGURE 1. Topology of the SMES converter.

of this method must be further improved. Reference [20] proposed a proportional resonant control method with effective harmonic suppression ability; however, the significant gain variation was found to affect the control result when the frequency of the AC component was offset. Passivity-based control (PBC), which is a nonlinear control method proposed by Romeo Ortega, has been widely applied to the PWM rectifier and other controlled objects [21]–[24]. The PBC method elucidates the law of energy flow in the nonlinear system by considering the interconnection structure of the system, thereby allowing the energy of the controlled system to be distributed according to the expectation, and the state variables are convergent to the equilibrium position. Therefore, the PBC method has the characteristics of fast response ability, strong robustness and clear physical meaning. According to the different modeling methods, the PBC method can be divided into two types: those based on an Euler-Lagrange (EL) model and those based on a port-controlled Hamiltonian (PCH) model. For PBC using EL models, the Lagrange structure of the system may be broken when the energy function is constructed; therefore, the stability of the system cannot be guaranteed. For PBC using PCH models, both damping injection and energy shaping can be easily conducted, and the controlled system can rapidly reach the steady state [25], [26]. There is currently a lack of research on the control strategy for the energy storage converter of SMES during network unbalance; therefore, it is important to study the PBC method of SMES under the unbalanced voltage condition.

The significant contribution of this study is the possibility to control the active and reactive power independently in a SMES system under the unbalanced voltage condition. First, the mathematical models and PCH models of SMES in positive and negative sequences are established. Second, the PBC method of SMES during network unbalance based on the PCH model is proposed to eliminate the nonlinearity of the energy storage converter. Third, the stability of the controller is analyzed according to the ''second method'' of Lyapunov. Finally, the effectiveness of the proposed control strategy is verified by simulation.

II. DYNAMICAL MODEL OF SMES SYSTEMS

Fig. 1 shows the topology of the SMES converter. In Fig. 1, u_a, u_b, and u_c represent the grid-side voltage; u_{1a}, u_{1b}, and u_{1c} represent the input voltage of the SMES converter; R and L represent the value of the AC-side resistance and inductor, respectively; i_a, i_b, and i_c represent the input current of the SMES converter; C represents the value of the DC-side capacitor; U_{dc} represents the DC-side voltage; L_{sc} corresponds to the inductance value of the superconducting magnet; and i_{sc} represents the current flowing through the magnet.

The mathematical model of the AC-side converter of the SMES in the abc reference frame can be expressed as

$$\begin{cases} L\dfrac{\mathrm{d}i_a}{\mathrm{d}t} = -Ri_a - S_a U_{dc} + u_{ga} \\ L\dfrac{\mathrm{d}i_b}{\mathrm{d}t} = -Ri_b - S_b U_{dc} + u_{gb} \\ L\dfrac{\mathrm{d}i_c}{\mathrm{d}t} = -Ri_c - S_c U_{dc} + u_{gc} \end{cases} \tag{1}$$

Using the $\alpha\beta$ reference frame via Clarke's transformation, these differential equations are presented as follows:

$$\begin{cases} u_\alpha = Ri_\alpha + L\dfrac{\mathrm{d}i_\alpha}{\mathrm{d}t} + u_{1\alpha} \\ u_\beta = Ri_\beta + L\dfrac{\mathrm{d}i_\beta}{\mathrm{d}t} + u_{1\beta} \end{cases} \tag{2}$$

where $u_{1\alpha} = S_\alpha U_{dc}$, and $u_{1\beta} = S_\beta U_{dc}$.

The symmetric component method specifies that the excitation of each sequence component produces a response in the respective sequence component only. All the electromagnetic variables can be decomposed into positive- and negative-sequence components. Thus, these variables can be expressed based on the positive- and negative-sequence components in the positive and negative synchronous reference frame using Park's transformation. The method mentioned in [27], referred to as delayed signal cancellation (DSC), is used to obtain the positive- and negative-sequence components of the three-phase quantities.

The positive- and negative-sequence models of the AC-side converter can be expressed as

$$\begin{cases} u^{p}_{gd+} = Ri^{p}_{gd+} + L\dfrac{\mathrm{d}i^{p}_{gd+}}{\mathrm{d}t} - \omega Li^{p}_{gq+} + u^{p}_{1gd+} \\ u^{p}_{gq+} = Ri^{p}_{gq+} + L\dfrac{\mathrm{d}i^{p}_{gq+}}{\mathrm{d}t} + \omega Li^{p}_{gd+} + u^{p}_{1gq+} \end{cases} \tag{3}$$

$$\begin{cases} u^{n}_{gd-} = Ri^{n}_{gd-} + L\dfrac{\mathrm{d}i^{n}_{gd-}}{\mathrm{d}t} + \omega Li^{n}_{gq-} + u^{n}_{1gd-} \\ u^{n}_{gq-} = Ri^{n}_{gq-} + L\dfrac{\mathrm{d}i^{n}_{gq-}}{\mathrm{d}t} - \omega Li^{n}_{gd-} + u^{n}_{1gq-} \end{cases} \tag{4}$$

where u^{p}_{gd+}, u^{p}_{gq+}, u^{p}_{1gd+}, u^{p}_{1gq+}, i^{p}_{gd+} and i^{p}_{gq+} represent the positive-sequence components of the grid-side voltage, input voltage of the converter and input current of the converter in the synchronous dq reference frame, respectively. And u^{n}_{gd-}, u^{n}_{gq-}, u^{n}_{1gd-}, u^{n}_{1gq-}, i^{n}_{gd-} and i^{n}_{gq-} represent the negative-sequence components of the grid-side voltage, input voltage of the converter and input current of the converter in the synchronous dq reference frame, respectively. The above positive- and negative-sequence components can be easily obtained by using the DSC method.

The mathematical model of the chopper can be expressed by introducing the duty cycle D of S_7 and S_8 as

$$\begin{cases} C(\mathrm{d}U_{\mathrm{dc}})/\mathrm{d}t = i_{\mathrm{dc}} - D^* i_{\mathrm{sc}} \\ L_{\mathrm{sc}}(\mathrm{d}i_{\mathrm{sc}})/\mathrm{d}t = -R_{\mathrm{sc}} i_{\mathrm{sc}} + D^* U_{\mathrm{dc}} \end{cases} \tag{5}$$

where D^* represents the average duty cycle of the chopper, namely, $D^* = 2D - 1$; R_{sc} and L_{sc} represent the resistance value and inductance value of the superconducting magnet, respectively, and R_{sc} is taken as zero in this study.

III. ANALYSIS OF THE CONTROL TARGET

In [18], the active and reactive power from the network to the energy storage converter can be expressed as

$$\begin{cases} P = P_0 + P_{2\sin}\sin(2\omega t) + P_{2\cos}\cos(2\omega t) \\ Q = Q_0 + Q_{2\sin}\sin(2\omega t) + Q_{2\cos}\cos(2\omega t) \end{cases} \tag{6}$$

where P_0 and Q_0 represent the DC component of the active and reactive power, respectively; $P_{\sin 2}$ and $P_{\cos 2}$ represent the double-frequency oscillations of the active power; $Q_{\sin 2}$ and $Q_{\cos 2}$ represent the double-frequency oscillations of the reactive power.

After coordinating the equations by using the DSC method, P (i.e., P_0, $P_{\sin 2}$, and $P_{\cos 2}$) and Q (i.e., Q_0, $Q_{\sin 2}$, and $Q_{\cos 2}$) can be given by

$$\begin{bmatrix} P_0 \\ P_{2\sin} \\ P_{2\cos} \\ Q_0 \\ Q_{2\sin} \\ Q_{2\cos} \end{bmatrix} = \frac{3}{2} \begin{bmatrix} u^{\mathrm{p}}_{\mathrm{gd}+} & u^{\mathrm{p}}_{\mathrm{gq}+} & u^{\mathrm{n}}_{\mathrm{gd}-} & u^{\mathrm{n}}_{\mathrm{gq}-} \\ u^{\mathrm{n}}_{\mathrm{gq}-} & -u^{\mathrm{n}}_{\mathrm{gd}-} & -u^{\mathrm{p}}_{\mathrm{gq}+} & u^{\mathrm{p}}_{\mathrm{gd}+} \\ u^{\mathrm{n}}_{\mathrm{gd}-} & u^{\mathrm{n}}_{\mathrm{gq}-} & u^{\mathrm{p}}_{\mathrm{gd}+} & u^{\mathrm{p}}_{\mathrm{gq}+} \\ u^{\mathrm{p}}_{\mathrm{gq}+} & -u^{\mathrm{p}}_{\mathrm{gd}+} & u^{\mathrm{n}}_{\mathrm{gq}-} & -u^{\mathrm{n}}_{\mathrm{gd}-} \\ -u^{\mathrm{n}}_{\mathrm{gd}-} & -u^{\mathrm{n}}_{\mathrm{gq}-} & u^{\mathrm{p}}_{\mathrm{gd}+} & u^{\mathrm{p}}_{\mathrm{gq}+} \\ u^{\mathrm{n}}_{\mathrm{gq}-} & -u^{\mathrm{n}}_{\mathrm{gd}-} & u^{\mathrm{p}}_{\mathrm{gq}+} & -u^{\mathrm{p}}_{\mathrm{gd}+} \end{bmatrix} \times \begin{bmatrix} i^{\mathrm{p}}_{\mathrm{gd}+} \\ i^{\mathrm{p}}_{\mathrm{gq}+} \\ i^{\mathrm{n}}_{\mathrm{gd}-} \\ i^{\mathrm{n}}_{\mathrm{gq}-} \end{bmatrix} \tag{7}$$

Under unbalanced network condition, we obtain both the DC components of active and reactive power and the second-harmonic components of active and reactive power. In light of the grid requirements, the SMES can be controlled to achieve one of the following targets:

Target I: Constant output active power, where the active power of the converter contains only the DC component.

Target II: Constant output reactive power, where the reactive power of the converter contains only the DC component.

Target III: To ensure balanced total currents from the SMES into the network, the output current contains no negative-sequence current.

For Target I, to remove the oscillations in the active power of the converter, based on the 1st to 4th rows in equation (7), the equations can be obtained as

$$\begin{bmatrix} P_0 \\ P_{2\sin} \\ P_{2\cos} \\ Q_0 \end{bmatrix} = \frac{3}{2} \begin{bmatrix} u^{\mathrm{p}}_{\mathrm{gd}+} & u^{\mathrm{p}}_{\mathrm{gq}+} & u^{\mathrm{n}}_{\mathrm{gd}-} & u^{\mathrm{n}}_{\mathrm{gq}-} \\ u^{\mathrm{n}}_{\mathrm{gq}-} & -u^{\mathrm{n}}_{\mathrm{gd}-} & -u^{\mathrm{p}}_{\mathrm{gq}+} & u^{\mathrm{p}}_{\mathrm{gd}+} \\ u^{\mathrm{n}}_{\mathrm{gd}-} & u^{\mathrm{n}}_{\mathrm{gq}-} & u^{\mathrm{p}}_{\mathrm{gd}+} & u^{\mathrm{p}}_{\mathrm{gq}+} \\ u^{\mathrm{p}}_{\mathrm{gq}+} & -u^{\mathrm{p}}_{\mathrm{gd}+} & u^{\mathrm{n}}_{\mathrm{gq}-} & -u^{\mathrm{n}}_{\mathrm{gd}-} \end{bmatrix} \times \begin{bmatrix} i^{\mathrm{p}}_{\mathrm{gd}+} \\ i^{\mathrm{p}}_{\mathrm{gq}+} \\ i^{\mathrm{n}}_{\mathrm{gd}-} \\ i^{\mathrm{n}}_{\mathrm{gq}-} \end{bmatrix} \tag{8}$$

Because the double-frequency oscillations ($P_{\sin 2}$ and $P_{\cos 2}$) in the active power must be zero, the value of the reference current can be solved as

$$\begin{cases} {i^{\mathrm{p}}_{\mathrm{gd}+}}^* = \dfrac{2}{3}\left(\dfrac{u^{\mathrm{p}}_{\mathrm{gd}+}}{D_1}P_0 + \dfrac{u^{\mathrm{p}}_{\mathrm{gq}+}}{D_2}Q_0\right), \\ {i^{\mathrm{p}}_{\mathrm{gq}+}}^* = \dfrac{2}{3}\left(\dfrac{u^{\mathrm{p}}_{\mathrm{gq}+}}{D_1}P_0 - \dfrac{u^{\mathrm{p}}_{\mathrm{gd}+}}{D_2}Q_0\right) \\ {i^{\mathrm{n}}_{\mathrm{gd}-}}^* = \dfrac{2}{3}\left(-\dfrac{u^{\mathrm{n}}_{\mathrm{gd}-}}{D_1}P_0 + \dfrac{u^{\mathrm{n}}_{\mathrm{gq}-}}{D_2}Q_0\right), \\ {i^{\mathrm{n}}_{\mathrm{gq}-}}^* = \dfrac{2}{3}\left(-\dfrac{u^{\mathrm{n}}_{\mathrm{gq}-}}{D_1}P_0 - \dfrac{u^{\mathrm{n}}_{\mathrm{gd}-}}{D_2}Q_0\right) \end{cases} \tag{9}$$

where P_0 and Q_0 represent the DC component of the active and reactive power, respectively, and also represent the power reference of SMES: $D_1 = {u^{\mathrm{p}}_{\mathrm{gd}+}}^2 + {u^{\mathrm{p}}_{\mathrm{gq}+}}^2 - {u^{\mathrm{n}}_{\mathrm{gd}-}}^2 - {u^{\mathrm{n}}_{\mathrm{gq}-}}^2$, and $D_2 = {u^{\mathrm{p}}_{\mathrm{gd}+}}^2 + {u^{\mathrm{p}}_{\mathrm{gq}+}}^2 + {u^{\mathrm{n}}_{\mathrm{gd}-}}^2 + {u^{\mathrm{n}}_{\mathrm{gq}-}}^2$; and ${i^{\mathrm{p}}_{\mathrm{gd}+}}^*$, ${i^{\mathrm{p}}_{\mathrm{gq}+}}^*$, ${i^{\mathrm{n}}_{\mathrm{gd}-}}^*$, ${i^{\mathrm{n}}_{\mathrm{gq}-}}^*$ represent the positive-sequence components of the input current references in the synchronous dq reference frame.

For Target II, to remove the oscillations in the reactive power of the converter, based on the 1st and 4th to 6th rows in equation (7), the following equations can be obtained:

$$\begin{bmatrix} P_0 \\ Q_0 \\ Q_{2\sin} \\ Q_{2\cos} \end{bmatrix} = \frac{3}{2} \begin{bmatrix} u^{\mathrm{p}}_{\mathrm{gd}+} & u^{\mathrm{p}}_{\mathrm{gq}+} & u^{\mathrm{n}}_{\mathrm{gd}-} & u^{\mathrm{n}}_{\mathrm{gq}-} \\ u^{\mathrm{p}}_{\mathrm{gq}+} & -u^{\mathrm{p}}_{\mathrm{gd}+} & u^{\mathrm{n}}_{\mathrm{gq}-} & -u^{\mathrm{n}}_{\mathrm{gd}-} \\ -u^{\mathrm{n}}_{\mathrm{gd}-} & -u^{\mathrm{n}}_{\mathrm{gq}-} & u^{\mathrm{p}}_{\mathrm{gd}+} & u^{\mathrm{p}}_{\mathrm{gq}+} \\ u^{\mathrm{n}}_{\mathrm{gq}-} & -u^{\mathrm{n}}_{\mathrm{gd}-} & u^{\mathrm{p}}_{\mathrm{gq}+} & -u^{\mathrm{p}}_{\mathrm{gd}+} \end{bmatrix} \times \begin{bmatrix} i^{\mathrm{p}}_{\mathrm{gd}+} \\ i^{\mathrm{p}}_{\mathrm{gq}+} \\ i^{\mathrm{n}}_{\mathrm{gd}-} \\ i^{\mathrm{n}}_{\mathrm{gq}-} \end{bmatrix} \tag{10}$$

Because the double-frequency oscillations ($Q_{\sin 2}$ and $Q_{\cos 2}$) in the reactive power must be zero, the value of the reference

current can be solved as

$$\begin{cases} {i_{\mathrm{gd+}}^{\mathrm{p}}}^{*} = \dfrac{2}{3}\left(\dfrac{u_{\mathrm{gd+}}^{\mathrm{p}}}{D_2}P_0 + \dfrac{u_{\mathrm{gq+}}^{\mathrm{p}}}{D_1}Q_0\right), \\ {i_{\mathrm{gq+}}^{\mathrm{p}}}^{*} = \dfrac{2}{3}\left(\dfrac{u_{\mathrm{gq+}}^{\mathrm{p}}}{D_2}P_0 - \dfrac{u_{\mathrm{gd+}}^{\mathrm{p}}}{D_1}Q_0\right) \\ {i_{\mathrm{gd-}}^{\mathrm{n}}}^{*} = \dfrac{2}{3}\left(\dfrac{u_{\mathrm{gd-}}^{\mathrm{n}}}{D_2}P_0 - \dfrac{u_{\mathrm{gq-}}^{\mathrm{n}}}{D_1}Q_0\right), \\ {i_{\mathrm{gq-}}^{\mathrm{n}}}^{*} = \dfrac{2}{3}\left(\dfrac{u_{\mathrm{gq-}}^{\mathrm{n}}}{D_2}P_0 + \dfrac{u_{\mathrm{gd-}}^{\mathrm{n}}}{D_1}Q_0\right) \end{cases} \tag{11}$$

For Target III, to remove the negative sequence current of the converter, based on the 1st and 4th rows in equation (7), the following equations can be obtained:

$$\begin{bmatrix} P_0 \\ Q_0 \end{bmatrix} = \frac{3}{2}\begin{bmatrix} u_{\mathrm{gd+}}^{\mathrm{p}} & u_{\mathrm{gq+}}^{\mathrm{p}} & u_{\mathrm{gd-}}^{\mathrm{n}} & u_{\mathrm{gq-}}^{\mathrm{n}} \\ u_{\mathrm{gq+}}^{\mathrm{p}} & -u_{\mathrm{gd+}}^{\mathrm{p}} & u_{\mathrm{gq-}}^{\mathrm{n}} & -u_{\mathrm{gd-}}^{\mathrm{n}} \end{bmatrix}\begin{bmatrix} i_{\mathrm{gd+}}^{\mathrm{p}} \\ i_{\mathrm{gq+}}^{\mathrm{p}} \\ 0 \\ 0 \end{bmatrix} \tag{12}$$

Because the negative sequence current ($i_{\mathrm{gd-}}^{\mathrm{n}}$ and $i_{\mathrm{gq-}}^{\mathrm{n}}$) must be zero, the value of the reference current can be solved as

$$\begin{cases} {i_{\mathrm{gd+}}^{\mathrm{p}}}^{*} = \dfrac{2}{3}\left(\dfrac{u_{\mathrm{gd+}}^{\mathrm{p}}P_0 + u_{\mathrm{gq+}}^{\mathrm{p}}Q_0}{{u_{\mathrm{gd+}}^{\mathrm{p}}}^2 + {u_{\mathrm{gq+}}^{\mathrm{p}}}^2}\right), \\ {i_{\mathrm{gq+}}^{\mathrm{p}}}^{*} = \dfrac{2}{3}\left(\dfrac{u_{\mathrm{gq+}}^{\mathrm{p}}P_0 + u_{\mathrm{gd+}}^{\mathrm{p}}Q_0}{{u_{\mathrm{gd+}}^{\mathrm{p}}}^2 + {u_{\mathrm{gq+}}^{\mathrm{p}}}^2}\right) \\ {i_{\mathrm{gd-}}^{\mathrm{n}}}^{*} = 0, \quad {i_{\mathrm{gq-}}^{\mathrm{n}}}^{*} = 0 \end{cases} \tag{13}$$

IV. CONTROL DESIGN

A. PCH MODELS OF THE SMES SYSTEM

The positive-sequence model of the AC-side converter described by Equation (3) is written as follows:

$$\boldsymbol{L}_{\mathrm{gp}}\dot{\boldsymbol{q}}_{\mathrm{gp}} + \boldsymbol{C}_{\mathrm{gp}}\boldsymbol{q}_{\mathrm{gp}} + \boldsymbol{R}_{\mathrm{gp}}\boldsymbol{q}_{\mathrm{gp}} = \boldsymbol{u}_{\mathrm{gp}} \tag{14}$$

where

$$\boldsymbol{L}_{\mathrm{gp}} = \begin{bmatrix} L & 0 \\ 0 & L \end{bmatrix}, \quad \boldsymbol{q}_{\mathrm{gp}} = \begin{bmatrix} i_{\mathrm{gd+}}^{\mathrm{p}} \\ i_{\mathrm{gq+}}^{\mathrm{p}} \end{bmatrix},$$
$$\boldsymbol{C}_{\mathrm{gp}} = \begin{bmatrix} 0 & -\omega L \\ \omega L & 0 \end{bmatrix}, \quad \boldsymbol{R}_{\mathrm{gp}} = \begin{bmatrix} R & 0 \\ 0 & R \end{bmatrix},$$
$$\boldsymbol{u}_{\mathrm{gp}} = \begin{bmatrix} u_{\mathrm{gd+}}^{\mathrm{p}} - u_{1\mathrm{gd+}}^{\mathrm{p}} \\ u_{\mathrm{gq+}}^{\mathrm{p}} - u_{1\mathrm{gq+}}^{\mathrm{p}} \end{bmatrix}.$$

The energy function of the AC-side converter of SMES is defined as

$$H_{\mathrm{gp}} = \boldsymbol{q}_{\mathrm{gp}}^{\mathrm{T}}\boldsymbol{L}_{\mathrm{gp}}\boldsymbol{q}_{\mathrm{gp}}/2 \tag{15}$$

Therefore,

$$\frac{\partial H_{\mathrm{gp}}}{\partial \boldsymbol{q}_{\mathrm{gp}}} = \begin{bmatrix} L & 0 \\ 0 & L \end{bmatrix}\begin{bmatrix} i_{\mathrm{gd+}}^{\mathrm{p}} \\ i_{\mathrm{gq+}}^{\mathrm{p}} \end{bmatrix} = \boldsymbol{L}_{\mathrm{gp}}\boldsymbol{q}_{\mathrm{gp}} \tag{16}$$

$$\boldsymbol{q}_{\mathrm{gp}} = \boldsymbol{L}_{\mathrm{gp}}^{-1}\left(\partial H_{\mathrm{gp}}/\partial \boldsymbol{q}_{\mathrm{gp}}\right) \tag{17}$$

By using (14), $\dot{\boldsymbol{q}}_{\mathrm{gp}}$ can be calculated as

$$\dot{\boldsymbol{q}}_{\mathrm{gp}} = -\boldsymbol{L}_{\mathrm{gp}}^{-1}\boldsymbol{C}_{\mathrm{gp}}\boldsymbol{L}_{\mathrm{gp}}^{-1}\frac{\partial H_{\mathrm{gp}}}{\partial \boldsymbol{q}_{\mathrm{gp}}} - \boldsymbol{L}_{\mathrm{gp}}^{-1}\boldsymbol{R}_{\mathrm{gp}}\boldsymbol{L}_{\mathrm{gp}}^{-1} + \boldsymbol{L}_{\mathrm{gp}}^{-1}\boldsymbol{u}_{\mathrm{gp}} \tag{18}$$

The positive-sequence PCH model of the AC-side converter can be described as

$$\begin{cases} \dot{\boldsymbol{q}}_{\mathrm{gp}} = \left[\boldsymbol{J}_{\mathrm{gp}} - \boldsymbol{\Re}_{\mathrm{gp}}\right]\dfrac{\partial H_{\mathrm{gp}}}{\partial \boldsymbol{q}_{\mathrm{gp}}} + \boldsymbol{g}_{\mathrm{gp}}\boldsymbol{u}_{\mathrm{gp}} \\ \boldsymbol{y}_{\mathrm{gp}} = \boldsymbol{g}_{\mathrm{gp}}^{\mathrm{T}}\dfrac{\partial H_{\mathrm{gp}}}{\partial \boldsymbol{q}_{\mathrm{gp}}} \end{cases} \tag{19}$$

where $\boldsymbol{J}_{\mathrm{gp}}$ represents the internal structure matrix, which reflects the internal energy conversion structure, and $\boldsymbol{\Re}_{\mathrm{gp}}$ represents the damping matrix, which reflects the energy dissipation characteristics.

Additionally, $\boldsymbol{J}_{\mathrm{gp}} = -L_{\mathrm{gp}}^{-1}\boldsymbol{C}_{\mathrm{gp}}L_{\mathrm{gp}}^{-1} = -\boldsymbol{J}_{\mathrm{gp}}^{\mathrm{T}}$, $\boldsymbol{\Re}_{\mathrm{gp}} = L_{\mathrm{gp}}^{-1}\boldsymbol{R}_{\mathrm{gp}}L_{\mathrm{gp}}^{-1} = \boldsymbol{\Re}_{\mathrm{gp}}^{\mathrm{T}} > 0$, and $\boldsymbol{g}_{\mathrm{gp}} = L_{\mathrm{gp}}^{-1}$.

By differentiating the energy function of the AC-side converter with respect to time, $\dot{H}_{\mathrm{gp}}$ can be calculated as

$$\dot{H}_{\mathrm{gp}} = \boldsymbol{q}_{\mathrm{gp}}^{\mathrm{T}}\boldsymbol{L}_{\mathrm{gp}}\dot{\boldsymbol{q}}_{\mathrm{gp}} = \boldsymbol{q}_{\mathrm{gp}}^{\mathrm{T}}\boldsymbol{L}_{\mathrm{gp}}\boldsymbol{g}_{\mathrm{gp}}\boldsymbol{u}_{\mathrm{gp}} - \boldsymbol{q}_{\mathrm{gp}}^{\mathrm{T}}\boldsymbol{L}_{\mathrm{gp}}\boldsymbol{\Re}_{\mathrm{gp}}\boldsymbol{L}_{\mathrm{gp}}\boldsymbol{q}_{\mathrm{gp}} \tag{20}$$

Using the integration method, the change of the system energy can be expressed as

$$\begin{aligned} H_{\mathrm{gp}}(t) - H_{\mathrm{gp}}(0) &= \int_0^t \boldsymbol{q}_{\mathrm{gp}}^{\mathrm{T}}\boldsymbol{L}_{\mathrm{gp}}\boldsymbol{g}_{\mathrm{gp}}\boldsymbol{u}_{\mathrm{gp}}\mathrm{d}\tau \\ &\quad - \int_0^t \boldsymbol{q}_{\mathrm{gp}}^{\mathrm{T}}\boldsymbol{L}_{\mathrm{gp}}\boldsymbol{\Re}_{\mathrm{gp}}\boldsymbol{L}_{\mathrm{gp}}\boldsymbol{q}_{\mathrm{gp}}\mathrm{d}\tau \\ &= \int_0^t \boldsymbol{q}_{\mathrm{gp}}^{\mathrm{T}}\boldsymbol{L}_{\mathrm{gp}}\boldsymbol{g}_{\mathrm{gp}}\boldsymbol{u}_{\mathrm{gp}}\mathrm{d}\tau - \int_0^t Q_{\mathrm{gp}}\mathrm{d}\tau \\ &< \int_0^t \boldsymbol{q}_{\mathrm{gp}}^{\mathrm{T}}\boldsymbol{L}_{\mathrm{gp}}\boldsymbol{g}_{\mathrm{gp}}\boldsymbol{u}_{\mathrm{gp}}\mathrm{d}\tau \end{aligned} \tag{21}$$

where $Q_{\mathrm{gp}} = \boldsymbol{q}_{\mathrm{gp}}^{\mathrm{T}}\boldsymbol{L}_{\mathrm{gp}}\boldsymbol{\Re}_{\mathrm{gp}}\boldsymbol{L}_{\mathrm{gp}}\boldsymbol{q}_{\mathrm{gp}} = L^2R({i_{\mathrm{gd+}}}^2 + {i_{\mathrm{gd-}}}^2) > 0$.

Therefore, we find that the energy stored by the system is less than the supplied energy, indicating that the positive-sequence model of the AC-side converter is strictly passive.

In the same manner, the negative-sequence PCH model of the AC-side converter can be described as

$$\begin{cases} \dot{\boldsymbol{q}}_{\mathrm{gn}} = \left[\boldsymbol{J}_{\mathrm{gn}} - \boldsymbol{\Re}_{\mathrm{gn}}\right]\dfrac{\partial H_{\mathrm{gn}}}{\partial \boldsymbol{q}_{\mathrm{gn}}} + \boldsymbol{g}_{\mathrm{gn}}\boldsymbol{u}_{\mathrm{gn}} \\ \boldsymbol{y}_{\mathrm{gn}} = \boldsymbol{g}_{\mathrm{gn}}^{\mathrm{T}}\dfrac{\partial H_{\mathrm{gn}}}{\partial \boldsymbol{q}_{\mathrm{gn}}} \end{cases} \tag{22}$$

Similarly, it can be proved that the negative-sequence model of the AC-side converter is strictly passive.

The energy function of the DC-side chopper of the SMES is defined as

$$H_{\mathrm{sc}} = \left(C{U_{\mathrm{dc}}}^2 + L_{\mathrm{sc}}{i_{\mathrm{sc}}}^2\right)\Big/2 \tag{23}$$

The state variables are defined as

$$\boldsymbol{q}_{\mathrm{sc}} = [C\ U_{\mathrm{dc}}\ L_{\mathrm{sc}}i_{\mathrm{sc}}]^{\mathrm{T}} \tag{24}$$

The PCH model of the DC-side chopper of the SMES can be described as

$$\begin{cases} \dot{\boldsymbol{q}}_{\mathrm{sc}} = [\boldsymbol{J}_{\mathrm{sc}} - \boldsymbol{\Re}_{\mathrm{sc}}] \dfrac{\partial H_{\mathrm{sc}}}{\partial \boldsymbol{q}_{\mathrm{sc}}} + \boldsymbol{g}_{\mathrm{sc}} \boldsymbol{u}_{\mathrm{sc}} \\ \boldsymbol{y}_{\mathrm{sc}} = \boldsymbol{g}_{\mathrm{sc}}^{\mathrm{T}} \dfrac{\partial H_{\mathrm{sc}}}{\partial \boldsymbol{q}_{\mathrm{sc}}} \end{cases} \tag{25}$$

where $\boldsymbol{J}_{\mathrm{sc}} = \begin{bmatrix} 0 & -D^* \\ D^* & 0 \end{bmatrix}$, $\boldsymbol{\Re}_{\mathrm{sc}} = \begin{bmatrix} 0 & 0 \\ 0 & 0 \end{bmatrix}$, $\boldsymbol{g}_{\mathrm{sc}} = \begin{bmatrix} 1 & 0 \end{bmatrix}^{\mathrm{T}}$ and $\boldsymbol{u}_{\mathrm{sc}} = i_{\mathrm{dc}}$

Due to the dissipation of energy, the energy stored by the magnetic field is less than the energy supplied by the AC-side converter, indicating that the model of the DC-side chopper is also strictly passive.

B. PBC METHOD OF THE SMES SYSTEM

The expected energy function of the positive-sequence model is defined as

$$H_{\mathrm{gpd}} = \boldsymbol{q}_{\mathrm{gpe}}^{\mathrm{T}} \boldsymbol{L}_{\mathrm{gp}} \boldsymbol{q}_{\mathrm{gpe}} / 2 \tag{26}$$

where $\boldsymbol{q}_{\mathrm{gpe}} = \boldsymbol{q}_{\mathrm{gp}} - \boldsymbol{q}_{\mathrm{gp}}^*$; $\boldsymbol{q}_{\mathrm{gp}}^*$ represents the reference value of the positive-sequence current of the converter, and $\boldsymbol{q}_{\mathrm{gp}}^* = \begin{bmatrix} i_{\mathrm{gd}+}^{\mathrm{p}} & i_{\mathrm{gq}+}^{\mathrm{p}} \end{bmatrix}^{\mathrm{T}}$.

Because of the conservation of the new internal structure matrix and the old internal structure matrix structure, the injected internal structure matrix and injected dissipation matrix of the AC-side converter are determined as

$$\boldsymbol{J}_{\mathrm{gpa}} = \boldsymbol{L}_{\mathrm{gp}}^{-1} \begin{bmatrix} J_{11} & -J_{12} \\ J_{12} & J_{22} \end{bmatrix} \boldsymbol{L}_{\mathrm{gp}}^{-1}, \quad \boldsymbol{\Re}_{\mathrm{gpa}} = \begin{bmatrix} r_1 & 0 \\ 0 & r_2 \end{bmatrix} \tag{27}$$

where the injected internal structure matrix satisfies the requirement of anti-symmetric matrix ($\boldsymbol{J}_{\mathrm{gpa}} = -\boldsymbol{J}_{\mathrm{gpa}}^{\mathrm{T}}$); r_1 and r_2 are the defined positive damping variables. The injected dissipation matrix also satisfies the condition of the positive-definite matrix ($\boldsymbol{\Re}_{\mathrm{gp}} = \boldsymbol{\Re}_{\mathrm{gp}}^{\mathrm{T}} > 0$).

Because $\frac{\partial H_{\mathrm{gp}}}{\partial \boldsymbol{q}_{\mathrm{gp}}} = \boldsymbol{L}_{\mathrm{gp}} \boldsymbol{q}_{\mathrm{gp}}$ and $\frac{\partial H_{\mathrm{gpd}}}{\partial \boldsymbol{q}_{\mathrm{gp}}} = \boldsymbol{L}_{\mathrm{gp}} \boldsymbol{q}_{\mathrm{gpe}}$, $\partial H_{\mathrm{gpa}} / \partial \boldsymbol{q}_{\mathrm{gp}}$ can be calculated as

$$\frac{\partial H_{\mathrm{gpa}}}{\partial \boldsymbol{q}_{\mathrm{gp}}} = \frac{\partial H_{\mathrm{gpd}}}{\partial \boldsymbol{q}_{\mathrm{gp}}} - \frac{\partial H_{\mathrm{gp}}}{\partial \boldsymbol{q}_{\mathrm{gp}}} = -\boldsymbol{L}_{\mathrm{gp}} \boldsymbol{q}_{\mathrm{gp}}^* \tag{28}$$

$\frac{\partial H_{\mathrm{gpd}}}{\partial \boldsymbol{q}_{\mathrm{gp}}} = \boldsymbol{L}_{\mathrm{gp}} \boldsymbol{q}_{\mathrm{gpe}} = 0$ and $\frac{\partial H_{\mathrm{gpd}}^2}{\partial \boldsymbol{q}_{\mathrm{gp}}^2} = \boldsymbol{L}_{\mathrm{gp}}$ is easily found at the equilibrium point $\boldsymbol{q}_{\mathrm{gp}}^*$; therefore, the expected Hamilton energy function H_{gpd} is minimized at the equilibrium point $\boldsymbol{q}_{\mathrm{gp}}^*$.

The energy-matching equation [28] of the positive-sequence model of the SMES converter can be expressed as

$$\left[\boldsymbol{J}_{\mathrm{gpd}} - \boldsymbol{\Re}_{\mathrm{gpd}}\right] \frac{\partial H_{\mathrm{gpa}}}{\partial \boldsymbol{q}_{\mathrm{gp}}} + \left[\boldsymbol{J}_{\mathrm{gpa}} - \boldsymbol{\Re}_{\mathrm{gpa}}\right] \frac{\partial H_{\mathrm{gp}}}{\partial \boldsymbol{q}_{\mathrm{gp}}} = \boldsymbol{g}_{\mathrm{gp}} \boldsymbol{u}_{\mathrm{gp}} \tag{29}$$

By solving the equation (29), the control law of positive-sequence model of the SMES converter can be written as

$$\boldsymbol{u}_{\mathrm{gp}} = \boldsymbol{g}_{\mathrm{gp}}^{-1} \left[\left(\boldsymbol{J}_{\mathrm{gpa}} - \boldsymbol{\Re}_{\mathrm{gpa}} \right) \boldsymbol{L}_{\mathrm{gp}} \boldsymbol{q}_{\mathrm{gp}} + \left(\boldsymbol{J}_{\mathrm{gpd}} - \boldsymbol{\Re}_{\mathrm{gpd}} \right) \boldsymbol{L}_{\mathrm{gp}} \boldsymbol{q}_{\mathrm{gp}}^* \right] \tag{30}$$

where $\boldsymbol{J}_{\mathrm{gpd}} = \boldsymbol{J}_{\mathrm{gp}} + \boldsymbol{J}_{\mathrm{gpa}}$; $\boldsymbol{\Re}_{\mathrm{gpd}} = \boldsymbol{\Re}_{\mathrm{gp}} + \boldsymbol{\Re}_{\mathrm{gpa}}$.

In the same manner, the control law of the negative-sequence model of the SMES converter can be written as

$$\boldsymbol{u}_{\mathrm{gn}} = \boldsymbol{g}_{\mathrm{gn}}^{-1} \left[\left(\boldsymbol{J}_{\mathrm{gna}} - \boldsymbol{\Re}_{\mathrm{gna}} \right) \boldsymbol{L}_{\mathrm{gn}} \boldsymbol{q}_{\mathrm{gn}} + \left(\boldsymbol{J}_{\mathrm{gnd}} - \boldsymbol{\Re}_{\mathrm{gnd}} \right) \boldsymbol{L}_{\mathrm{gn}} \boldsymbol{q}_{\mathrm{gn}}^* \right] \tag{31}$$

where $\boldsymbol{J}_{\mathrm{gnd}} = \boldsymbol{J}_{\mathrm{gn}} + \boldsymbol{J}_{\mathrm{gna}}$; $\boldsymbol{\Re}_{\mathrm{gnd}} = \boldsymbol{\Re}_{\mathrm{gn}} + \boldsymbol{\Re}_{\mathrm{gna}}$.

By substituting variables into (30) and (31), the control law of the AC-side converter can be described as

$$\begin{cases} u_{1\mathrm{gd}+}^{\mathrm{p}} = \left(r_1 L^2 - J_{11}\right) \left(i_{\mathrm{gd}+}^{\mathrm{p}} - {i_{\mathrm{gd}+}^{\mathrm{p}}}^* \right) \\ \quad - R {i_{\mathrm{gd}+}^{\mathrm{p}}}^* + J_{12} \left(i_{\mathrm{gq}+}^{\mathrm{p}} - {i_{\mathrm{gq}+}^{\mathrm{p}}}^* \right) + \omega L {i_{\mathrm{gq}+}^{\mathrm{p}}}^* + u_{\mathrm{gd}+}^{\mathrm{p}} \\ u_{1\mathrm{gq}+}^{\mathrm{p}} = \left(r_2 L^2 - J_{11}\right) \left(i_{\mathrm{gq}+}^{\mathrm{p}} - {i_{\mathrm{gq}+}^{\mathrm{p}}}^* \right) \\ \quad - R {i_{\mathrm{gq}+}^{\mathrm{p}}}^* - J_{12} \left(i_{\mathrm{gd}+}^{\mathrm{p}} - {i_{\mathrm{gd}+}^{\mathrm{p}}}^* \right) - \omega L {i_{\mathrm{gd}+}^{\mathrm{p}}}^* + u_{\mathrm{gq}+}^{\mathrm{p}} \\ u_{1\mathrm{gd}-}^{\mathrm{n}} = \left(r_1 L^2 - J_{11}\right) \left(i_{\mathrm{gd}-}^{\mathrm{n}} - {i_{\mathrm{gd}-}^{\mathrm{n}}}^* \right) \\ \quad - R {i_{\mathrm{gd}-}^{\mathrm{n}}}^* + J_{12} \left(i_{\mathrm{gq}-}^{\mathrm{n}} - {i_{\mathrm{gq}-}^{\mathrm{n}}}^* \right) - \omega L {i_{\mathrm{gq}-}^{\mathrm{n}}}^* + u_{\mathrm{gd}-}^{\mathrm{n}} \\ u_{1\mathrm{gq}-}^{\mathrm{n}} = \left(r_2 L^2 - J_{11}\right) \left(i_{\mathrm{gq}-}^{\mathrm{n}} - {i_{\mathrm{gq}-}^{\mathrm{n}}}^* \right) \\ \quad - R {i_{\mathrm{gq}-}^{\mathrm{n}}}^* - J_{12} \left(i_{\mathrm{gd}-}^{\mathrm{n}} - {i_{\mathrm{gd}-}^{\mathrm{n}}}^* \right) + \omega L {i_{\mathrm{gd}-}^{\mathrm{n}}}^* + u_{\mathrm{gq}-}^{\mathrm{n}} \end{cases} \tag{32}$$

The expected energy function of the DC-side chopper is defined as

$$H_{\mathrm{scd}} = \frac{1}{2} L_{\mathrm{sc}} \left(i_{\mathrm{sc}} - i_{\mathrm{sc}}^* \right)^2 + \frac{1}{2} C (U_{\mathrm{dc}} - U_{\mathrm{dc}}^*)^2 \tag{33}$$

where i_{sc}^* is the current reference of the magnet, which is an intermediate variable that can be eliminated.

The injected internal structure matrix and injected dissipation matrix of the chopper are respectively determined as

$$\boldsymbol{J}_{\mathrm{sca}} = \begin{bmatrix} 0 & 0 \\ 0 & 0 \end{bmatrix}, \quad \boldsymbol{\Re}_{\mathrm{sca}} = \begin{bmatrix} r_{\mathrm{a}} & 0 \\ 0 & r_{\mathrm{b}} \end{bmatrix} \tag{34}$$

where r_{a} and r_{b} are the defined positive damping variables; $\boldsymbol{J}_{\mathrm{scd}} = \boldsymbol{J}_{\mathrm{sc}} + \boldsymbol{J}_{\mathrm{sca}}$, and $\boldsymbol{\Re}_{\mathrm{scd}} = \boldsymbol{\Re}_{\mathrm{sc}} + \boldsymbol{\Re}_{\mathrm{sca}}$.

The state variable of the chopper at the equilibrium point is $\boldsymbol{q}_{\mathrm{sc}}^* = [C U_{\mathrm{dc}}^* L_{\mathrm{sc}} i_{\mathrm{sc}}^*]^{\mathrm{T}}$, and the expected Hamilton energy function H_{scd} should have a minimum value at the equilibrium point $\boldsymbol{q}_{\mathrm{sc}}^*$.

The energy-matching equation of the DC-side chopper of SMES can be expressed as

$$[\boldsymbol{J}_{\mathrm{scd}} - \boldsymbol{\Re}_{\mathrm{scd}}] \frac{\partial H_{\mathrm{sca}}}{\partial \boldsymbol{q}_{\mathrm{sc}}} + [\boldsymbol{J}_{\mathrm{sca}} - \boldsymbol{\Re}_{\mathrm{sca}}] \frac{\partial H_{\mathrm{sc}}}{\partial \boldsymbol{q}_{\mathrm{sc}}} = \boldsymbol{g}_{\mathrm{sc}} \boldsymbol{u}_{\mathrm{sc}} \tag{35}$$

By solving equation (35), the control law of the DC-side chopper of the SMES can be written as

$$\begin{cases} i_{\mathrm{sc}}^* = \dfrac{r_{\mathrm{b}} i_{\mathrm{sc}} + \sqrt{(i_{\mathrm{sc}} r_{\mathrm{b}})^2 + 4 r_{\mathrm{b}} U_{\mathrm{dc}}^* [i_{\mathrm{dc}} + r_{\mathrm{a}} (U_{\mathrm{dc}} - U_{\mathrm{dc}}^*)]}}{2 r_{\mathrm{b}}} \\ D^* = \dfrac{-r_{\mathrm{b}} i_{\mathrm{sc}} + \sqrt{(r_{\mathrm{b}} i_{\mathrm{sc}})^2 + 4 r_{\mathrm{b}} U_{\mathrm{dc}}^* [i_{\mathrm{dc}} + r_{\mathrm{a}} (U_{\mathrm{dc}} - U_{\mathrm{dc}}^*)]}}{2 U_{\mathrm{dc}}^*} \end{cases} \tag{36}$$

To verify the stability of the proposed passivity-based controller, the "second method" of Lyapunov is used. Because the H_{gpd} of the positive-sequence model is a positive-definite

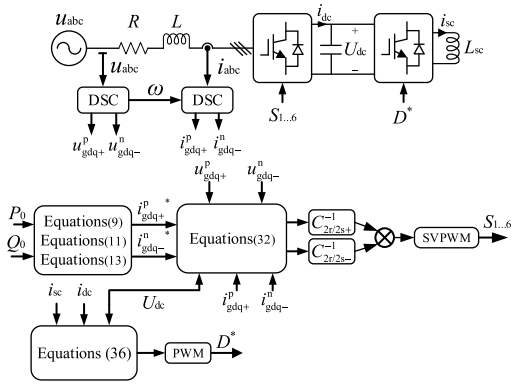

FIGURE 2. Block diagram for the proposed SMES control strategy.

function, this model is directly selected as the Lyapunov function for analysis. The stability of the controller can be judged by the derivative of H_{gpd} given as follows:

$$\frac{\mathrm{d}H_{\mathrm{gpd}}}{\mathrm{d}t} = \left[\nabla H_{\mathrm{gpd}}\right]^{\mathrm{T}} \dot{\boldsymbol{q}}^{\bullet}_{\mathrm{gp}} = \left[\nabla H_{\mathrm{gpd}}\right]^{\mathrm{T}} \left[\boldsymbol{J}_{\mathrm{gpd}} - \boldsymbol{R}_{\mathrm{gpd}}\right] \nabla H_{\mathrm{gpd}} \tag{37}$$

$\boldsymbol{J}_{\mathrm{gpd}}$ is an anti-symmetric matrix ($\boldsymbol{J}_{\mathrm{gpd}} = -\boldsymbol{J}^{\mathrm{T}}_{\mathrm{gpd}}$); therefore, $[\nabla H_{\mathrm{gpd}}]^{\mathrm{T}} \boldsymbol{J}_{\mathrm{gpd}} \nabla H_{\mathrm{gpd}} \equiv 0$, and $\boldsymbol{R}_{\mathrm{gpd}}$ is a positive-definite matrix. As a result, the derivative of H_{gpd} can be expressed as

$$\frac{\mathrm{d}H_{\mathrm{gpd}}}{\mathrm{d}t} = -\left[\nabla H_{\mathrm{gpd}}\right]^{\mathrm{T}} \boldsymbol{R}_{\mathrm{gpd}} \nabla H_{\mathrm{gpd}} < 0 \tag{38}$$

Equation (38) implies that the derivative of H_{gpd} is negative, i.e., H_{gpd} is non-positive and has a value of zero only at the balance position. Therefore, the positive-sequence controller exhibits asymptotical stability at the equilibrium position. Moreover, when $|\boldsymbol{q}_{\mathrm{gp}}|| \rightarrow \infty$, $H_{\mathrm{gpd}} \rightarrow \infty$, that is, the positive-sequence controller can achieve large-scale asymptotic stability near the equilibrium position.

Similarly, the negative-sequence controller and the chopper controller can also achieve large-scale asymptotic stability near the equilibrium position.

Fig. 2 shows the block diagram for the proposed SMES control strategy.

V. SIMULATION ANALYSIS

The simulation model is implemented using SIMULINK with MATLAB R2016a and executed using a PC with an Intel Core (TM) i7-6700K CPU (4.00 GHz) and 32 GB of RAM running Windows 10.

To verify the effectiveness of the proposed positive- and negative-sequence PBC method for the SMES system during network unbalance, a simulation analysis is performed on the MATLAB/ SIMULINK platform. To illustrate the advantages of proposed PBC method, a comparison is made between the PBC method and the traditional positive- and negative-sequence PI control method.

The model parameters are shown in Table I.

TABLE 1. Parameters for simulation.

Parameter	Value	Unit	Parameter	Value	Unit
Source voltage (line to line)	380	V	Magnet inductance	5	H
Grid frequency	50	Hz	Running current	100-600	A
AC-side inductance	2	mH	DC-side voltage	1200	V
DC-side capacitor	4000	μF	Maximal stored energy	0.9	MJ

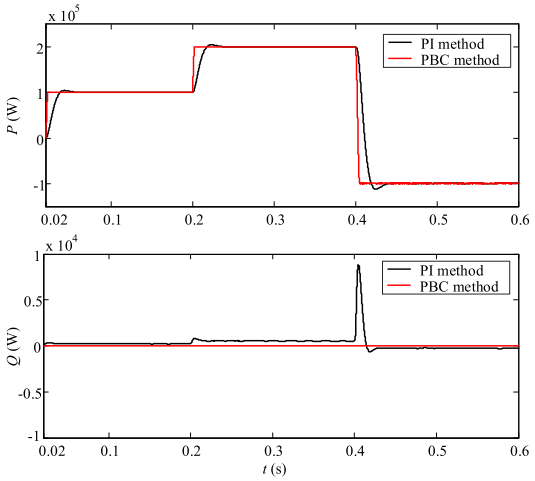

FIGURE 3. Power response curves of the SMES system.

Case 1: Since the proposed PBC method is also applicable to the voltage balance condition, the dynamic response capability of the system under the voltage balance condition is first tested. In this example, the step-change active power references of SMES system are set; specifically, the references active power 0.1 MW, 0.2 MW and −0.1 MW are applied to the SMES system at the times of 0 s, 0.2 s and 0.4 s, respectively. To achieve the unit power factor control of the SMES system during charging and discharging, the reference value of the reactive power is set as zero. Fig. 3 shows a comparison of the power response performance between the PI method and the PBC method.

The PBC method tracks the power references in a short time without overshoot, which effectively overcomes the tradeoff between the overshoot and the adjustment time of the PI controller. In contrast to the conventional PI method, the PBC method does not require adjustment of numerous parameters, thereby efficiently reducing the design complexity of the control system. In the process of a step change of active power, the reactive power is almost unaffected, thereby proving that the PBC method can effectively realize independent control between the active power and reactive power.

Fig. 4 shows the waveforms of the d-axis current and the q-axis current of the converter. The PBC method is found to have excellent characteristics in the transient state and the steady state.

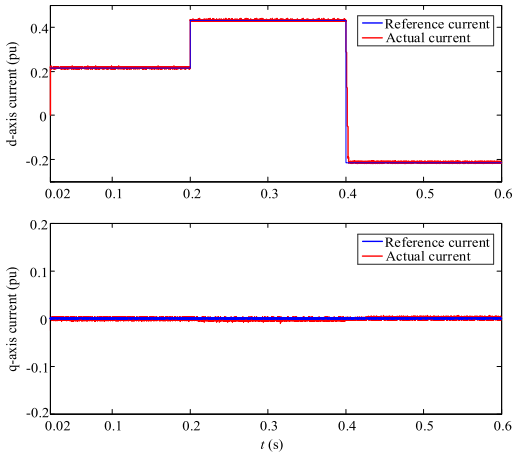

FIGURE 4. Waveforms of the d-axis current and q-axis current of the converter.

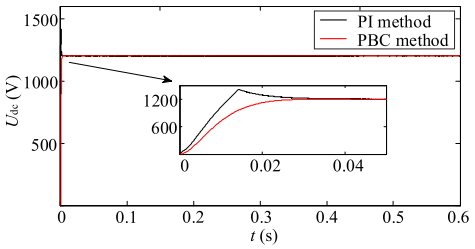

FIGURE 5. Waveforms of the DC-side voltage of the converter.

Fig. 5 shows a performance comparison between controlling the DC-side voltage with the PI method and with the PBC method. The PBC method stabilizes the DC-side voltage at the reference value rapidly and accurately.

Case 2: To illustrate the superiority of the proposed PBC method under the unbalanced voltage condition, two types of control strategies, namely, the traditional PI method and the PBC method, were adopted to the SMES system. Network unbalance was created by dropping the voltage of phase A to 80% during the period of 0.1 s to 0.4 s. The SMES selects different control targets at different time periods. The control target was initially set to Target I and was then switched to Target II at 0.2 s and to Target III at 0.3 s.

Fig. 6 shows a comparison of the output current of the SMES between the PI method and the PBC method. The output current of PI method with the three control targets exhibits prominent ripple, and the PBC method can effectively eliminate the ripple of the output current. Fig. 7 shows the spectral analysis diagram of the phase-A current using the fast Fourier transform from 0.3 s to 0.4 s; the PBC method is found to reduce the total harmonic distortion (THD) of the output current, thereby effectively improving the output characteristic of the SMES converter.

Fig. 8 shows the waveforms of the active and reactive power of the SMES converters under the two control strategies. The measured pulsations of active power and reactive power to the fundamental components for various control

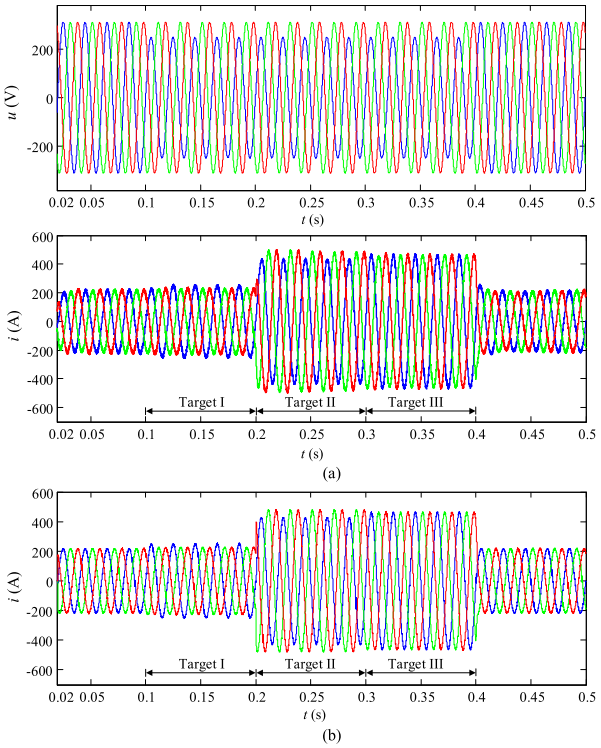

FIGURE 6. Waveforms of the grid voltage and output current of SMES. (a) PI method. (b) PBC method.

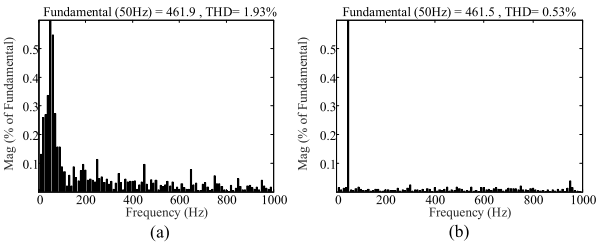

FIGURE 7. Harmonic component of the Phase-A current from 0.3 s to 0.4 s.

TABLE 2. Comparison of the operation results of the two control methods under various control objectives.

Control method		Target 1	Target 2	Target 3
PI method	Active power P (%)	±1.47	±15.25	±6.25
	Reactive power Q (%)	±14.64	±1.15	±7.05
PBC method	Active power P (%)	±0.12	±6.01	±3.25
	Reactive power Q (%)	±5.94	±0.07	±3.15

targets are compared in Table II. Both the PI method and the PBC method remove the oscillations in the controlled target. However, the steady-state performance of the PI method is poorer than that of the PBC method, and the transient process of the PI method exhibits much worse performance, with an apparent overshoot.

Relative to the conventional PI method, the reactive power pulsation component was reduced from ±14.64% to ±5.94%

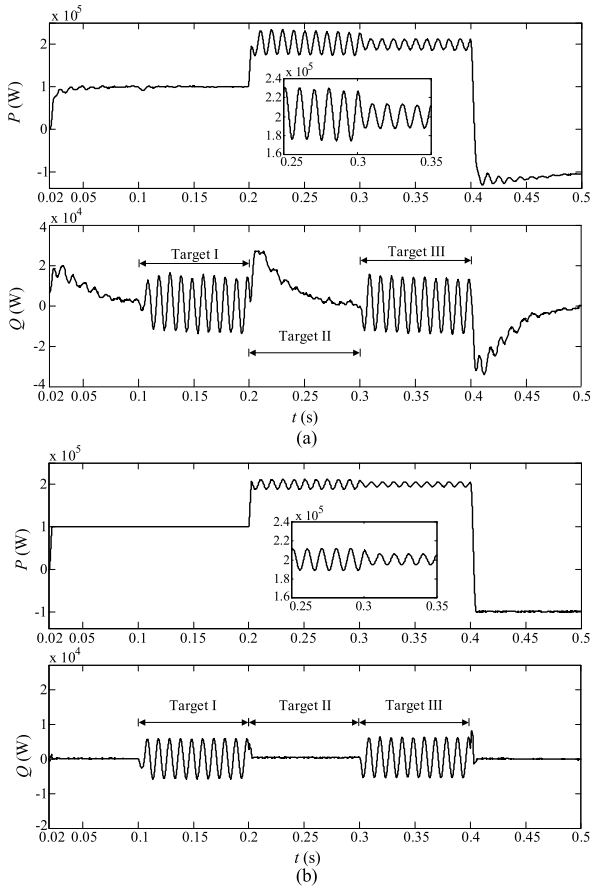

FIGURE 8. Simulated results with various control targets.

using Target I for the SMES. The active power oscillation was decreased from ±15.25% to ±6.01%, and the reactive power oscillations was reduced from ±1.15% to ±0.07% by selecting Target II. For Target III, the active power oscillation was decreased from ±6.25% to ±3.25%, and the reactive power oscillations was suppressed to ±3.15%. Generally, by adopting the proposed PBC method, the adjusting time and overshoot of active and reactive power and the harmonic of the output current are much less than those of the PI method.

VI. CONCLUSIONS

We have presented an analysis of a SMES system operating under unbalanced network conditions. A PCH model of the SMES system was established in the positive and negative sequence, and the PBC method for the SMES under unbalanced voltage condition was proposed. During this first stage of research, the accuracy of the research results was verified through simulations using MATLAB/SIMULINK. The conclusions of this study are as follows:

1) Under the unbalanced voltage condition, the passivity-based controller has low control complexity, strong robustness, few adjustable parameters and satisfactory performance in both the steady and dynamic states, thereby effectively overcoming the shortcomings of the conventional PI method and providing a new approach for improving the overall performance of SMES systems.

2) The SMES system with the designed PBC method can provide a timely response to suppress the oscillations caused by the unbalanced voltage and effectively reduce the THD of the AC-side current.

Because of the current hardware restrictions, future research will involve additional testing on the general performance of the proposed SMES system.

REFERENCES

[1] M. Jabir, H. A. Illias, S. Raza, and H. Mokhlis, "Intermittent smoothing approaches for wind power output: A review," *Energies*, vol. 10, no. 10, p. 1572, Oct. 2017.

[2] L. Chang, W. Zhang, S. Xu, and K. Spence, "Review on distributed energy storage systems for utility applications," *CPSS Trans. Power Electron. Appl.*, vol. 2, no. 4, pp. 267–276, Dec. 2017.

[3] L. Chen *et al.*, "SMES-battery energy storage system for the stabilization of a photovoltaic-based microgrid," *IEEE Trans. Appl. Supercond.*, vol. 28, no. 4, pp. 1–7, Jun. 2018.

[4] L. Chen *et al.*, "Conceptual design and evaluation of an HTS magnet for an SMES used in improving transient performance of a grid-connected PV system," *IEEE Trans. Appl. Supercond.*, vol. 28, no. 3, pp. 1–8, Apr. 2018.

[5] W. Guo *et al.*, "Development of a 1-MVA/1-MJ superconducting fault current limiter-magnetic energy storage system for LVRT capability enhancement and wind power smoothing," *IEEE Trans. Appl. Supercond.*, vol. 28, no. 4, pp. 1–5, Jun. 2018.

[6] J. Deng, J. Shi, Y. Liu, and Y. Tang, "Application of a hybrid energy storage system in the fast charging station of electric vehicles," *IET Generat., Transmiss. Distrib.*, vol. 10, no. 4, pp. 1092–1097, Mar. 2016.

[7] Z. X. Zheng, X. Y. Xiao, C. S. Li, Z. Chen, and Y. Zhang, "Performance evaluation of SMES system for initial and steady voltage sag compensations," *IEEE Trans. Appl. Supercond.*, vol. 26, no. 7, pp. 1–5, Oct. 2016.

[8] Z. Chen, X. Y. Xiao, C. S. Li, Y. Zhang, and Z. X. Zheng, "Study on unit commitment problem considering large-scale superconducting magnetic energy storage systems," *IEEE Trans. Appl. Supercond.*, vol. 26, no. 7, pp. 1–6, Oct. 2016.

[9] I. Ngamroo, "Optimization of SMES-FCL for augmenting FRT performance and smoothing output power of grid-connected DFIG wind turbine," *IEEE Trans. Appl. Supercond.*, vol. 26, no. 7, pp. 1–5, Oct. 2016.

[10] H. A. Hamed, A. A. F. Abdou, S. S. Acharya, M. S. E. Moursi, and E. E. El-Kholy, 'A novel dynamic switching table based direct power control strategy for grid connected converters," *IEEE Trans. Energy Convers.*, to be published, doi: 10.1109/TEC.2018.2795700.

[11] B. Saber, B. Abdelkader, B. Said, and B. Mansour, "Integral sliding mode control of four-leg DSTATCOM coupled with SMES unit," in *Proc. 5th Int. Conf. Elect. Eng.-Boumerdes (ICEE-B)*, Boumerdes, Algeria, Oct. 2017, pp. 1–6.

[12] Y. F. Tang, H. B. He, and C. X. Mu, "Superconducting magnetic energy storage based power system control using ADP," in *Proc. IEEE Int. Conf. Appl. Supercond. Electromagn. Devices (ASEMD)*, Shanghai, China, Nov. 2015, pp. 87–88.

[13] Y. Q. Xing, J. X. Jin, Y. L. Wang, B. X. Du, and S. C. Wang, "An electric vehicle charging system using an SMES implanted smart grid," *IEEE Trans. Appl. Supercond.*, vol. 26, no. 7, pp. 1–4, Oct. 2016.

[14] M. Zoghlami and F. Bacha, "Implementation of different strategies of direct power control," in *Proc. IREC2015 6th Int. Renew. Energy Congr.*, Sousse, Tunisia, Mar. 2015, pp. 1–6.

[15] S. C. Tan, Y. M. Lai, and C. K. Tse, "General design issues of sliding-mode controllers in DC-DC converters," *IEEE Trans. Ind. Electron.*, vol. 55, no. 3, pp. 1160–1174, Mar. 2008.

[16] P. Cheng and H. Nian, "Collaborative control of DFIG system during network unbalance using reduced-order generalized integrators," *IEEE Trans. Energy Convers.*, vol. 30, no. 2, pp. 453–464, Jun. 2015.

[17] C. A. Busada, S. G. Jorge, A. E. Leon, and J. A. Solsona, "Current controller based on reduced order generalized integrators for distributed generation systems," *IEEE Trans. Ind. Electron.*, vol. 59, no. 7, pp. 2898–2909, Jul. 2012.

[18] L. Xu, B. R. Andersen, and P. Cartwright, "VSC transmission operating under unbalanced AC conditions—Analysis and control design," *IEEE Trans. Power Del.*, vol. 20, no. 1, pp. 427–434, Jan. 2005.
[19] L. Xu and Y. Wang, "Dynamic modeling and control of DFIG-based wind turbines under unbalanced network conditions," *IEEE Trans. Power Syst.*, vol. 22, no. 1, pp. 314–323, Feb. 2007.
[20] G. Shen, X. Zhu, J. Zhang, and D. Xu, "A new feedback method for PR current control of LCL-filter-based grid-connected inverter," *IEEE Trans. Ind. Electron.*, vol. 57, no. 6, pp. 2033–2041, Jun. 2010.
[21] R. Ortega, A. J. Van der Schaft, I. Mareels, and B. Maschke, "Putting energy back in control," *IEEE Control Syst. Mag*, vol. 21, no. 2, pp. 18–33, Apr. 2001.
[22] R. Ortega and E. Garcia-Canseco, "Interconnection and damping assignment passivity-based control: A survey," *Eur. J. Control*, vol. 10, no. 5, pp. 432–450, 2004.
[23] D. Jeltsema, R. Ortega, and J. M. A. Scherpen, "An energy-balancing perspective of interconnection and damping assignment control of nonlinear systems," *Automatica*, vol. 40, no. 9, pp. 1643–1646, Sep. 2004.
[24] F. M. Serra, C. H. De Angelo, and D. G. Forchetti, "Interconnection and damping assignment control of a three-phase front end converter," *Int. J. Elect. Power Energy Syst.*, vol. 60, pp. 317–324, Sep. 2014.
[25] H. H. Song and Y. B. Qu, "Energy-based modelling and control of wind energy conversion system with DFIG," *Int. J. Control*, vol. 84, no. 2, pp. 281–292, Feb. 2011.
[26] J. Wang and H. Yin, "Passivity based controller design based on EL and PCHD Model," *Procedia Eng.*, vol. 15, pp. 33–37, Jan. 2011.
[27] J. Svensson, M. Bongiorno, and A. Sannino, "Practical implementation of delayed signal cancellation method for phase-sequence separation," *IEEE Trans. Power Del.*, vol. 22, no. 1, pp. 18–26, Jan. 2007.
[28] Y. B. Qu and H. H. Song, "Energy-based coordinated control of wind energy conversion system with DFIG," *Int. J. Control*, vol. 84, no. 12, pp. 2035–2045, Dec. 2011.

YONG LEI received the B.S. and M.S. degrees in electrical engineering from Southwest Jiaotong University, Chengdu, Sichuan, China, in 1989 and 1993, respectively, and the Ph.D. degree in mechanical manufacturing and its automation from Sichuan University, Chengdu, in 2002. He is currently a Professor with the College of Electrical Engineering and Information Technology, Sichuan University. His research interests include high-temperature superconducting techniques and intelligent measurement techniques.

XIAODONG LIN was born in Chengdu, Sichuan, in 1993. He received the B.S. degree in electrical engineering from Sichuan University, Chengdu, Sichuan, China, in 2016, where he is currently pursuing the M.S. degree in electrical engineering. His research interests include the control and optimization of hybrid energy storage systems and applied superconductivity.

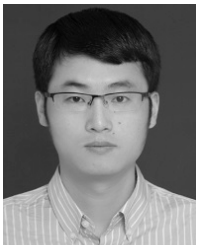

YINGWEI ZHU was born in Hubei, China, in 1982. He received the B.S. degree in electronic science and technology and the Ph.D. degree in theory of electrical engineering and new technology from Southwest Jiaotong University, Chengdu, China, in 2006 and 2011, respectively. He is currently an Associate Professor with the College of Electrical Engineering and Information Technology, Sichuan University. His major fields of research interests include superconducting magnetic energy storage, electromagnetic launch, and electromagnetic-field numerical simulation.